Data-Driven Feedback Linearization Control of Distributed Energy Resources using Sparse Regression

Javad Khazaei, *Senior Member, IEEE* and Ali Hosseinipour, *Student Member, IEEE*

***Abstract*—A complex physics-based modeling procedure and the uncertainty and confidentiality of internal parameters of distributed energy resources (DERs) motivate system identification tools for control purposes in smart grids. This paper develops a framework for data-driven nonlinear modeling and control of DERs using sparse identification of nonlinear dynamics (SINDy). Using the proposed data-driven model for closed-loop control, we demonstrate the effectiveness of a model-free design in stability analysis of DERs in smart grids. Feedback linearization control of DERs was chosen over conventional vector control in this research due to its superior capability of accounting for DER nonlinearities and weak AC grid integration. Compared with existing physics-based designs that heavily rely on knowing the detailed system dynamics or uninterpretable data-driven designs that rely on large historical data, the proposed model-free DER identification and control framework can accurately capture the dynamics of the DERs based on available measurements and provide guaranteed performance for black-start, weak AC grid integration, microgrid integration, and stability analysis. Real-time and offline simulations in addition to a detailed eigenvalue analysis are conducted to compare the effectiveness of the proposed data-driven approach with physics-based controllers.**

***Index Terms*—Sparse Identification of Nonlinear Dynamics (SINDy), Feedback Linearization, Distributed Energy Resource (DER).**

I. Introduction

Numerous inverter-based distributed energy resources (DERs) are currently being integrated into the energy grid. According to the electric reliability council of Texas (ERCOT), the grid may become inoperable once DER penetration passes 80% of annual energy demand. In addition, although these DERs are nonlinear in nature, they are typically controlled by cascaded linear regulators, which do not guarantee performance when the operating points of the system change, resulting in grid instability. For instance, a three-phase fault in July 2020 reduced the output of a solar photovoltaic (PV) system in Southern California by approximately 1000 MW. According to the north American electric reliability corporation (NERC), the failure was caused by the instability of linear current regulators [1]. This shows a clear limitation of existing DER controllers that heavily rely on linear regulators and thus calls for advanced controllers that could provide more robustness and guaranteed stability for the integration of DERs to the grid. One of the key knowledge gaps in controlling DERs is the lack of robust controller designs that properly account for DERs nonlinear nature and can improve the grid dynamics without involving expensive controller redesigns/tuning as a result of numerous expansions in the power grid.

The stability issues of DERs in smart grids have received significant attention over the past decade. These studies can be categorized into a) stability analysis approaches [1]–[3], b) supplementary control design [4]–[6], and c) controller redesign [7]–[9]. These studies often suggest an operating range/controller gain to stabilize interactions, which might not be feasible when the system expands or if there are uncertainties/faults. As a result, advanced control techniques are needed to provide a wider operating range without the need for controller re-design. With nonlinear controllers, these barriers can be overcome and predictable performance can be achieved over a wide operating range. There have been several studies focused on the design of nonlinear controllers (i.e., sliding-mode control [10], model predictive control [11], and feedback linearization control [12], [13]) for inverter-based DERs to improve the grid resilience. While nonlinear controllers are robust, they require a detailed mathematical model of the system for guaranteed performance [14]–[16]. The question is, can we reduce the complexities of nonlinear control designs for DERs by solving the modeling challenges via machine learning?

Machine learning has recently provided new tools for predicting physics-based models of dynamical systems. Many approaches have been utilized for data-driven model identification of dynamics such as dynamic mode decomposition (DMD) [17], neural networks (NNs) [18], Koopman operator [19], and sparse identification of nonlinear dynamics (SINDy) [20]. In power systems application, several recent studies have focused on data-driven modeling using these approaches [21]–[26]. For example, dynamic mode decomposition was utilized in [21] for a microgrid control method that is delay tolerant, or Koopman operator was utilized in [23] to identify the dynamics of generators for state estimation purposes. As another example, a data-driven approach using machine learning tools was proposed in [25] to identify the lifetime of lithium-ion batteries. Among these methods, dynamic mode decomposition heavily relies on a linear dynamics assumption, but can handle high-dimensional data. Neural-network-based approaches require a large amount of training data and are also infamous for not being interpretable [20], [27]. A Koopman operator connects dynamic mode decomposition

This research was in part under support from the National Science Foundation under Grant NSF-EPCN 2221784. J. Khazaei is with the Electrical and Computer Engineering department at Lehigh University, PA, USA. (E-mails:$jak921@lehigh.edu$ and $alh622@lehigh.edu$)

to nonlinear dynamics through an infinite dimensional linear operator. Under special circumstances and provided that a good measurement basis is selected, Koopman operator may converge to a finite dimensional space, which is not guaranteed for many systems [19], [28]. On the other hand, sparse identification uses the sparse regression technique to identify dominant dynamics of candidate functions, and has shown promise in accurately modeling the unknown dynamics of nonlinear systems [29], [30]. Among the major advantages of SINDy is its sparsity, which enables easy implementation, reduces the training time, results in an interpretable model, and provides an accurate formulation that outperforms other model identification techniques.

While the existing research shows the significant potential of SINDy in identifying nonlinear dynamics of dynamical systems, its application in DER control has not been reported yet. The paper aims to explore such a data-driven control framework by identifying the nonlinear dynamics of DERs using SINDy and utilizing the data-driven model for nonlinear control purposes in smart grids. In particular, the main contributions of the paper are listed as:

1- Many classical control techniques including feedback linearization require a detailed mathematical model of DERs in order to provide robustness and guaranteed performance. This paper addresses the heavy reliance of feedback linearization technique on physical models and instead utilize a data-driven model that is obtained exclusively from measurements for control design.
2- This paper utilizes sparse identification technique, which is a statistical machine learning framework leveraged for the model identification of nonlinear DERs in smart grids. The proposed method utilizes available measurements and a library of potential candidate functions without extensive training and is computationally robust unlike deep learning methods that require a large amount of data. The proposed data-driven framework reduces the complexity of state-of-the-art physics-based modeling and provides a scalable framework for DER control to resolve the grid stability issues.
3- Utilizing the obtained data-driven DER models for the nonlinear control of DERs via feedback linearization technique, which resolves the grid stability problems caused by classical linear controllers.
4- Detailed stability analysis of the proposed data-driven DER model under various grid strength conditions and sensitivity analysis of controller gains to test the robustness of the designed framework.
5- Evaluating the effectiveness of the proposed data-driven DER control framework in microgrid integration, weak AC grid integration, black-start conditions and real-time simulation using an OPAL-RT platform.

The rest of the paper is organized as follows: Section II formulates the converter modeling and Section III discusses the data-driven converter modeling using SINDy. Data-driven control design using feedback linearization theory is included in Section IV. Section V elaborates the case studies and results, and section VI concludes the paper.

II. Dynamic Modeling of the Converter

As Fig. 1 depicts a voltage source converter (VSC)-interfaced DER that is connected to the main grid through an LCL filter composed of L_c, r_c, and C_f. L_n and r_n represent the inductive and resistive parts of the grid impedance, respectively. Through the VSC, DC voltage (such as batteries or solar panels) is converted to AC, enabling the integration to the grid.

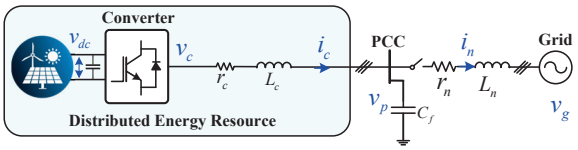

Fig. 1: Typical configuration of a grid-connected DER.

A. Modeling LCL Filter Dynamics

Assuming we have access to the measurements at the point of common coupling (PCC), the AC-side dynamics of the DER in dq frame can be expressed as [13]:

$$v_{cd} - v_{pd} + \omega_0 L_c i_{cq} = (L_c s + r_c) i_{cd} \quad (1)$$
$$v_{cq} - v_{pq} - \omega_0 L_c i_{cd} = (L_c s + r_c) i_{cq} \quad (2)$$
$$v_{pd} - v_{gd} + \omega_0 L_n i_{nq} = (L_n s + r_n) i_{nd} \quad (3)$$
$$v_{pq} - v_{gq} - \omega_0 L_n i_{nd} = (L_n s + r_n) i_{nq} \quad (4)$$
$$i_{cd} - i_{nd} + \omega_0 C_f v_{pq} = C_f s v_{pd} \quad (5)$$
$$i_{cq} - i_{nq} - \omega_0 C_f v_{pd} = C_f s v_{pq} \quad (6)$$

where s is the Laplace operator, ω_0 is the nominal frequency of the system, i.e., 377 rad/s, and v_{cd}, v_{cq}, i_{cd}, and i_{cq} are the dq-frame components of the converter output voltage and current, respectively. The dq-frame components of the voltage at the PCC and grid are denoted by v_{pd}, v_{pq}, v_{gd}, and v_{gq}, respectively. In addition, the dq-frame components of the grid current are expressed by i_{nd} and i_{nq}. The above equations can be written in a matrix form as:

$$\begin{bmatrix} \dot{i}_{cd} \\ \dot{i}_{cq} \\ \dot{v}_{pd} \\ \dot{v}_{pq} \\ \dot{i}_{nd} \\ \dot{i}_{nq} \end{bmatrix} = \begin{bmatrix} -\frac{r_c}{L_c} & \omega_0 & 0 & 0 & -\frac{1}{L_c} & 0 \\ -\omega_0 & -\frac{r_c}{L_c} & 0 & 0 & 0 & -\frac{1}{L_c} \\ 0 & 0 & -\frac{r_g}{L_g} & \omega_0 & \frac{1}{L_g} & 0 \\ 0 & 0 & -\omega_0 & -\frac{r_g}{L_g} & 0 & \frac{1}{L_g} \\ \frac{1}{C_f} & 0 & -\frac{1}{C_f} & 0 & 0 & \omega_0 \\ 0 & \frac{1}{C_f} & 0 & -\frac{1}{C_f} & -\omega_0 & 0 \end{bmatrix} \begin{bmatrix} i_{cd} \\ i_{cq} \\ v_{pd} \\ v_{pq} \\ i_{nd} \\ i_{nq} \end{bmatrix} + g(u)$$

$$g(u) = \begin{bmatrix} \frac{v_{cd}}{L_c} & \frac{v_{cq}}{L_c} & 0 & 0 & \frac{-v_{gd}}{L_g} & \frac{-v_{gq}}{L_g} \end{bmatrix}^T. \quad (7)$$

III. Model-Free Identification of DERs

Dynamical systems with few nonlinear terms are often studied using sparsity promoting techniques to identify candidate functions with the greatest impact on the system dynamics.

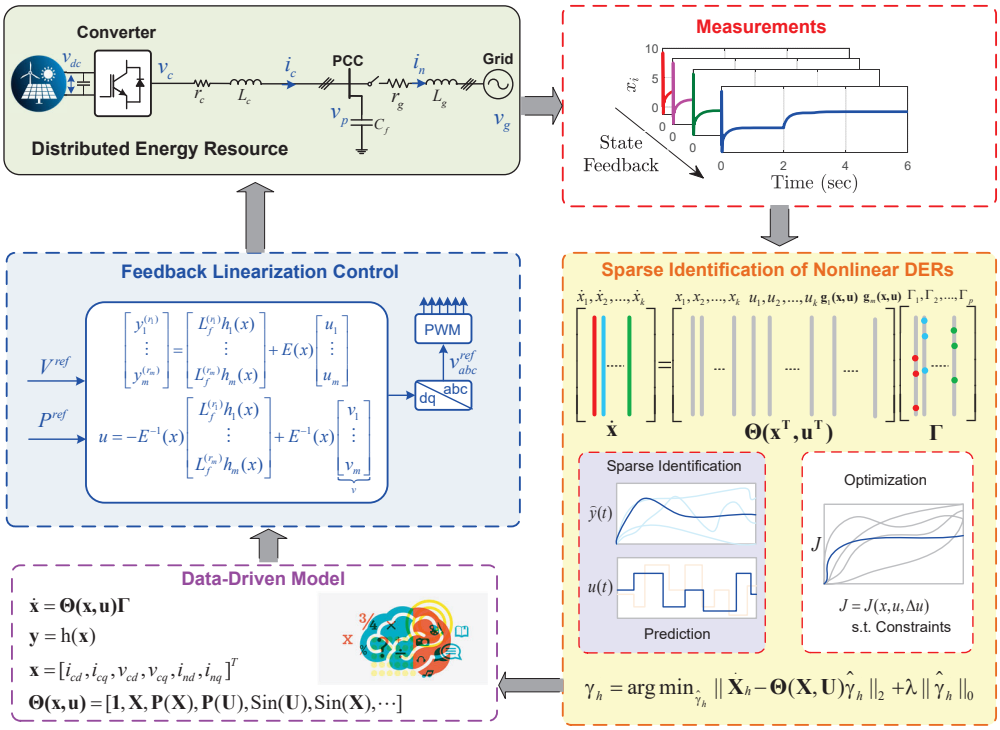

Fig. 2: Identified DER dynamics using SINDy.

Originally proposed in [29], SINDy utilizes a symbolic regression technique to identify nonlinear dynamics. The concept behind the sparse identification theory is that many real-world dynamical systems in form of $\dot{\mathbf{x}} = \mathrm{f}(\mathbf{x}, \mathbf{u})$ may have a few terms on the right-hand side. Therefore, following (7), the dynamics of a DER is expressed by $\dot{\mathbf{x}} = \mathbf{f}(\mathbf{x}) + \mathbf{g}(\mathbf{x})\mathbf{u}$, where $\mathbf{x}(t) \in \mathbb{R}^n$ denotes the state vector, $\mathbf{u}(t) \in \mathbb{R}^q$ is the input (control) vector, and $\mathbf{f}(\mathbf{x}(t), \mathbf{u}(t)) : \mathbb{R}^n \times \mathbb{R}^q \to \mathbb{R}^n$. The goal of SINDy is to reconstruct (7) from the available measurement. If our knowledge of the model is limited, we can utilize available measurements (voltages and currents at the PCC) to identify this model using SINDy and then utilize a data-driven model (which is almost identical to the physical model with slightly different parameters) for the control design. Therefore, the control design can be treated as a grey-box model, where the control gains are obtained from a data-driven model instead of a physical model.

A. Data Collection

First, the measurements are sampled at m intervals $t_1, t_2, \ldots, t_m$ and are arranged into a state matrix $\mathbf{X} \in \mathbb{R}^{n \times m}$, and input matrix $\mathbf{U} \in \mathbb{R}^{n \times m}$,

$$\mathbf{X} = \begin{bmatrix} | & | & & | \\ \mathbf{x}(t_1) & \mathbf{x}(t_2) & \ldots & \mathbf{x}(t_m) \\ | & | & & | \end{bmatrix} \tag{8}$$

$$\mathbf{U} = \begin{bmatrix} | & | & & | \\ \mathbf{u}(t_1) & \mathbf{u}(t_2) & \ldots & \mathbf{u}(t_m) \\ | & | & & | \end{bmatrix} \tag{9}$$

As derivative measurements in most systems cannot be observed, they can be approximated numerically from $\mathbf{X}$.

B. Estimating the Derivative Matrix $\dot{\mathbf{X}}$

Differential equations can be numerically solved using a difference approximation. Taylor series expansions can be used to approximate the derivatives of a smooth function in the neighborhood of point x. For smooth functions, the central difference approximation is more accurate. Therefore, following the central difference approximation concept, the $\dot{\mathbf{X}}$ can be obtained by:

$$\dot{\mathbf{X}} \approx \frac{\mathbf{X}(i+1) - \mathbf{X}(i-1)}{2h} \tag{10}$$

In the above formula, $\mathbf{X}(i)$ is the ith measurement vector and h is the sampling interval of the measurement system [31].

C. Sparse Identification of DER Dynamics

If limited knowledge of the DER dynamics is available (i.e., type of filter used is not known) or the impedance of the line connecting the inverter from PCC to the grid is not known, the DER dynamics can be expressed by a library of p candidate functions $\boldsymbol{\Theta}(\mathbf{X}, \mathbf{U}) \in \mathbb{R}^{n \times p}$. This library can include polynomials, monomials, or sinusoids in general that can represent any dynamical system of interest. It is known that the vector of measured derivatives, $\dot{\mathbf{X}}$, is a linear combination of columns in the candidate function library, which is observed by the entries of matrix $\boldsymbol{\Xi} \in \mathbb{R}^{p \times n}$ [29], i.e.,

$$\dot{\mathbf{X}} = \boldsymbol{\Theta}(\mathbf{X}, \mathbf{U})\boldsymbol{\Xi}. \tag{11}$$

$$\Theta(\mathbf{X},\mathbf{U}) = \begin{bmatrix} | & | & | & | & | & & | & | & | & \\ 1 & \mathbf{X} & \mathbf{U} & \mathbf{P_2}(\mathbf{X},\mathbf{U}) & \mathbf{P_3}(\mathbf{X},\mathbf{U}) & \dots & \sin(\mathbf{X},\mathbf{U}) & \cos(\mathbf{X},\mathbf{U}) & \sin(\mathbf{2}(\mathbf{X},\mathbf{U})) & \dots \\ | & | & | & | & | & & | & | & | & \end{bmatrix} \tag{12}$$

After estimating $\dot{\mathbf{X}}$ from the available state feedback using central difference approximation in (10), and having measured the control input data, $\mathbf{U}$, the candidate function library is built by including linear and nonlinear functions of the columns of $\mathbf{X}$ and $\mathbf{U}$ as shown in equation (12).

In (12), $\mathbf{P_i}(\mathbf{X},\mathbf{U})$ is a nonlinear combination of i-order polynomials of $\mathbf{X}$ and $\mathbf{U}$. For example, $\mathbf{P_3}(\mathbf{X},\mathbf{U})$ includes polynomials up to third order such as: $x_i x_j$, x_i^2, $x_i^2 x_j$, x_i^3, $x_i u_j$, $u_i^2 x_j$, $x_i^2 u_j$, and u_i^3. The unknown in (11) is a sparse matrix $\boldsymbol{\Xi}$, columns of which denote which candidate functions are active in the dynamics of the DER. Knowing the estimated derivatives $\dot{\mathbf{X}}$ and calculating $\boldsymbol{\Theta}(\mathbf{X},\mathbf{U})$ from available measurements, we can utilize the sparse regression theory to solve for the sparse matrix of coefficients, $\boldsymbol{\Xi}$. This is achieved by iteratively solving an optimization of the form:

$$\boldsymbol{\xi}_k = \arg\min_{\hat{\boldsymbol{\xi}}_k} ||\dot{\mathbf{X}}_k - \boldsymbol{\Theta}(\mathbf{X},\mathbf{U})\hat{\boldsymbol{\xi}}_k||_2 + \lambda_k ||\hat{\boldsymbol{\xi}}_k||_0 \tag{13}$$

where $\boldsymbol{\xi}_k$ is the k-th column of $\boldsymbol{\Xi}$ represented by $\boldsymbol{\xi}_k = \begin{bmatrix}\xi_1 & \xi_2 & \dots & \xi_p\end{bmatrix}^T$ and $\dot{\mathbf{X}}_k$ represents the k-th column of $\dot{\mathbf{X}}$. The L2 norm $||.||_2$ in the objective function in (13) tries to minimize the error between the actual derivatives $\dot{\mathbf{X}}$ and estimated derivatives $\dot{\mathbf{X}} = \boldsymbol{\Theta}(\mathbf{X},\mathbf{U})$ via an iterative least-squares optimization and the L0 norm $||.||_0$ tries to promote sparsity in the matrix of coefficients $\boldsymbol{\Xi}$ by minimizing its number of nonzero elements. In addition, a sparsity promoting hyperparameter λ_k is defined and tuned for kth column of $\dot{\mathbf{X}}$ imperially to result in the best estimation of the dynamics. The closer the λ_k is to zero, the less sparse the coefficient matrix $\boldsymbol{\Xi}$ is. It was recommended to approximately solve the optimization problem in (13) using the sequentially thresholded least squares estimation [27]. The method is originally proposed in [32], which is briefly explained in the following.

$$S^m = \left\{j \in [p] : \left|\xi_j^m\right| \geq \lambda_k\right\}, \quad m \geq 0 \tag{14}$$

$$\hat{\boldsymbol{\xi}}_k^0 = \boldsymbol{\Theta}(\mathbf{X},\mathbf{U})^\dagger \dot{\mathbf{X}}_k \tag{15}$$

$$\boldsymbol{\xi}_k^{m+1} = \underset{\hat{\boldsymbol{\xi}}_k \in \mathbb{R}^p : \text{supp}(\boldsymbol{\xi}_k) \subseteq S^m}{\text{argmin}} \|\dot{\mathbf{X}}_k - \boldsymbol{\Theta}(\mathbf{X},\mathbf{U})\hat{\boldsymbol{\xi}}_k\|_2, \tag{16}$$

where m is the iteration number, $\boldsymbol{\Theta}(\mathbf{X},\mathbf{U})^\dagger$ is the pseudo-inverse of $\boldsymbol{\Theta}(\mathbf{X},\mathbf{U})$ expressed as

$$\boldsymbol{\Theta}(\mathbf{X},\mathbf{U})^\dagger := [\boldsymbol{\Theta}(\mathbf{X},\mathbf{U})^T \boldsymbol{\Theta}(\mathbf{X},\mathbf{U})]^{-1} \boldsymbol{\Theta}(\mathbf{X},\mathbf{U})^T \tag{17}$$

and $\text{supp}(\boldsymbol{\xi}_k) := \{j \in [p] : \xi_j \neq 0\}$ is the support set of $\boldsymbol{\xi}_k$. The iterative approach for obtaining the sparse coefficients of the system dynamics using the SINDy method is listed in **Algorithm 1**. Applying the SINDy algorithm to the measurements of the DER, one can obtain the sparse coefficients matrix and identify the AC-side dynamics in the form of $\dot{\mathbf{X}} = \boldsymbol{\Theta}(\mathbf{X},\mathbf{U})$, which can be re-arranged into the original form represented by (7). To validate the effectiveness of the SINDy for identifying the DER dynamics in (7), time-domain simulations were carried out and the results are illustrated in Fig. 3. The collected data include the measurements of 6 states and 4 inputs, i.e., $x = [i_{cd}, i_{cq}, v_{pd}, v_{pq}, i_{nd}, i_{nq}]$ and inputs $v_{cd}, v_{cq}, v_{gd}, v_{gq}$ for 1.5 seconds with a sampling time of 50 microseconds (300,000 samples). Therefore, the size of $\mathbf{X}$ is $6 \times 300,000$ and the size of $\mathbf{U}$ is $4 \times 300,000$. By applying step changes to the control inputs v_{cd} and v_{cq}, accompanied by a Guassian noise with a zero mean and a variance of 5 V, the required data for training the sparse regression algorithm is acquired. The candidate function terms in $\boldsymbol{\Theta}(\mathbf{X},\mathbf{U})$ include polynomials of up to the 2nd degree and sinusoidal functions, i.e., u_i, x_i, $x_i x_j$, x_i^2, $x_i \cos x_j$, $x_i \sin x_j$, $u_i \cos x_j$, $u_i \sin x_j$. The identified coefficient matrix $\boldsymbol{\Xi}$ for the studied DER model is used to develop a data-driven model in MATLAB. As it will be shown later in the study, the obtained data-driven dynamics closely track the original states and the SINDy algorithms is shown to successfully identify the DER dynamics. The obtained data-driven dynamics will be used for control design purposes, which will be elaborated in the next section.

Algorithm 1 Sparse Regression Algorithm

Input: Measurements $\mathbf{X}, \mathbf{U}$
Input: Estimate derivatives $\dot{\mathbf{X}}$ using (10)
procedure SINDy ALGORITHM
$\Gamma = \Theta \backslash \dot{\mathbf{X}}$ (least-square solution)
  for k = 1 : 10 **do** (number of iterations)
    Set λ (sparsity promoting constant)
    $|\Xi| < \lambda \longrightarrow ind_{small}$
    $\Xi(ind_{small}) \longrightarrow 0$
    for k = 1 : n **do** (n dimension of state $\mathbf{X}$)
      $ind_{big} \neq ind_{small}(:,k)$
      $\Xi(ind_{big},k) = \Theta(:,ind_{big}) \backslash \dot{\mathbf{X}}(:,k)$
    end for
  end for
Output: sparse matrix Ξ

D. Impact of Number of Candidate Functions

To analyze the impact of number of candidate functions in the library $\boldsymbol{\Theta}(\mathbf{X},\mathbf{U})$ on prediction accuracy, a case study is presented in this section. First, only x_i and u_i terms are included in the model (i.e., $\boldsymbol{\Theta}(\mathbf{X},\mathbf{U}) = [x_1, \dots, x_6, u_1, \dots u_6]$), then the number of candidate functions were increased to 22 by adding $x_i u_j$ terms, i.e., $[x_1.u_1,\ x_1.u_2,\ x_1.u_3,\ x_1.u_4,\ x_1.u_5,\ x_2.u_1,\ x_2.u_2,\ x_2.u_3,\ x_2.u_4,\ x_2.u_5]$. Similarly, the number of functions were increased to 42 and 54 by adding more terms including x_i^2 (polynomials up to degree 2) and sinusoidal terms (i.e.,

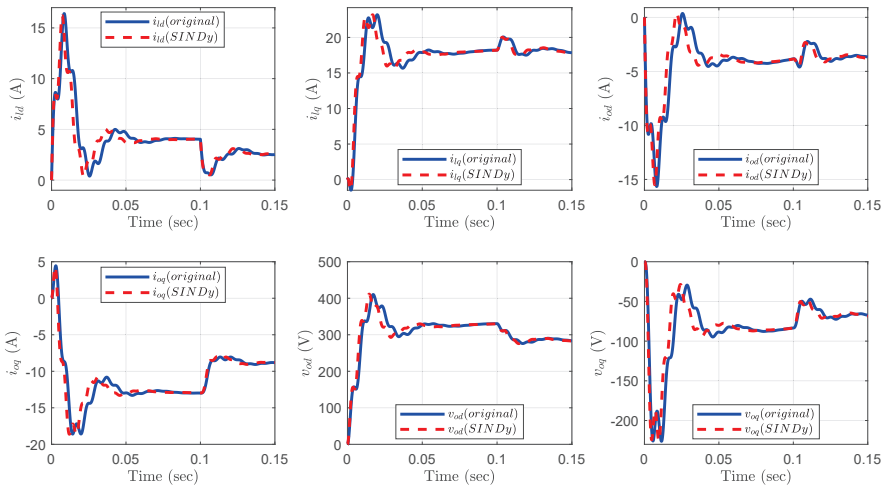

Fig. 3: Training results of SINDy to learn the dynamics of the DER.

$sin(x_i)$). It is noted that the hyperparameter λ has to be retuned when the number of candidate functions is increased. Fig. 4 depicts the normalized prediction error as a function of number of candidate functions. As it can be seen, by increasing the number of candidate functions, the prediction error increases. The results suggest that the best prediction is achieved when we have some knowledge about the possible terms in the dynamics in order to avoid the large number of candidate functions that can increase the prediction error. This is one of the challenges of utilizing SINDy for real-world problems that necessitates some background knowledge about the dynamics for better results. In the following analyses, we utilized 54 candidate functions to run the experiments.

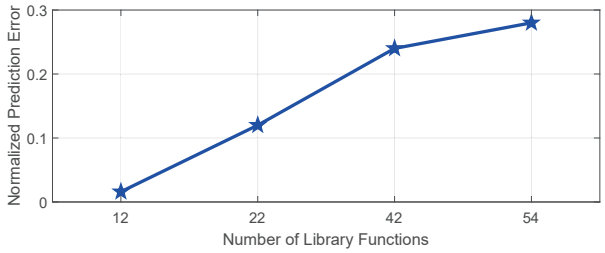

Fig. 4: Impact of number of library functions on prediction accuracy of DER models.

IV. Data-Driven Control Design

To avoid the stability challenges of linear regulators elaborated in the introduction section, we will design a data-driven nonlinear controller using feedback linearization theory, which has proven to be effective in improving the dynamic performance of DERs in various grid integration scenarios [13]. In this section, we will lay out the fundamentals of feedback linearization, followed by the development of control strategies. Readers are encouraged to refer to [33] for more information on the theory of feedback linearization technique.

A. Feedback Linearization Theory

To generalize the DER dynamics in (7) for various configurations, assume a multi-input multi-output (MIMO) dynamical system is represented by $\dot{\mathbf{x}} = f(\mathbf{x}) + g(\mathbf{x})\mathbf{u}$, where $\mathbf{x}$ is an n-dimensional state vector, $\mathbf{u} \in \mathbb{R}^m$ is the vector of control input, and $g(\mathbf{x})$ is a smooth matrix field on $\mathbb{R}^n$. In addition, the output dynamics is expressed as $\mathbf{y} = h(\mathbf{x})$, with $f(\mathbf{x})$ is a smooth vector field on $\mathbb{R}^n$, and $h(x)$ is a smooth output function. One should note that the DER model in (7) can easily be transformed into the standard MIMO model represented above. In feedback linearization control, to deal with the nonlinearities of the system, the output $\mathbf{y}$ will be differentiated repeatedly until at least one input variable u_i appears. For instance, repeated derivatives (also known as Lie derivatives) can be defined as [33]:

$$L_f^{(k)}h(\mathbf{x}) = L_f(L_f^{(k-1)}h(\mathbf{x}) = \frac{\partial L_f^{(k-1)}h(\mathbf{x})}{\partial \mathbf{x}} f(\mathbf{x}) \qquad (18)$$

where $L_f h(\mathbf{x})$ and $L_g h(\mathbf{x})$ are Lie derivatives of $h(\mathbf{x})$ and $g(\mathbf{x})$, respectively. If the input appears after r_m derivations of the output, then,

$$y_i^{(r_m)} = L_f^{(r_m)}h_i(\mathbf{x}) + \sum_{j=1}^{m} L_{g_j} L_f^{(r_m-1)}h_i(\mathbf{x})u_j, \qquad (19)$$

where $i = \{1, 2, \ldots, m\}$. The above equation can be written in a matrix form as:

$$\begin{bmatrix} y_1^{(r_1)} \\ \vdots \\ y_m^{(r_m)} \end{bmatrix} = \begin{bmatrix} L_f^{(r_1)}h_1(\mathbf{x}) \\ \vdots \\ L_f^{(r_m)}h_m(\mathbf{x}) \end{bmatrix} + E(\mathbf{x}) \begin{bmatrix} u_1 \\ \vdots \\ u_m \end{bmatrix} \qquad (20)$$

where

$$E(\mathbf{x}) = \begin{bmatrix} L_{g_1} L_f^{(r_1-1)}h_1(\mathbf{x}) & \ldots & L_{g_m} L_f^{(r_1-1)}h_1(\mathbf{x}) \\ \vdots & \ddots & \vdots \\ L_{g_1} L_f^{(r_m-1)}h_m(\mathbf{x}) & \ldots & L_{g_m} L_f^{(r_m-1)}h_m(\mathbf{x}) \end{bmatrix}$$

and $L_g L_f h(x) = \dfrac{\partial L_f h(\mathbf{x})}{\partial \mathbf{x}} g(\mathbf{x})$ and $L_f L_f h(\mathbf{x}) = L_f^2 h(\mathbf{x}) = \dfrac{\partial L_f h(\mathbf{x})}{\partial \mathbf{x}} f(\mathbf{x})$. The number of times that the output needs to be differentiated until the input $\mathbf{u}$ appears is called the relative degree of the system and is denoted by a vector relative degree $\mathbf{v_{rd}} = \{r_1,\ r_2,\ \ldots,\ r_m\}$ at an equilibrium point $\mathbf{x}_0$. According to [33], a solution can be found for choices of output functions $h_i(\mathbf{x}), i \in \{1, 2, \ldots, m\}$ if the total relative degree of the system, e.g., $\sum_{i=1}^{m} r_i$, is equal to the dimension of the system's state-space model n. In this condition, the control input can be designed by:

$$\mathbf{u} = -E^{-1}(\mathbf{x}) \begin{bmatrix} L_f^{(r_1)} h_1(\mathbf{x}) \\ \vdots \\ L_f^{(r_m)} h_m(\mathbf{x}) \end{bmatrix} + E^{-1}(\mathbf{x}) \underbrace{\begin{bmatrix} v_1 \\ \vdots \\ v_m \end{bmatrix}}_{\mathbf{v}} \tag{21}$$

where v is the new input vector to be designed to achieve a control objective, i.e., zero tracking error of $y_i^{ref} - y_i$ [33]. By replacing the control input from (21) in the MIMO model of the system, the system is converted to a linear decoupled closed-loop model represented by $y_k^{(r_k)} = v_k,\ k \in \{1, 2, ..., m\}$, which is written in a matrix form as:

$$\mathbf{y}^{(r)} = \begin{bmatrix} y_1^{(r_1)},\ \vdots,\ y_m^{(r_m)} \end{bmatrix}^T = \mathbf{v} = \begin{bmatrix} v_1,\ \vdots,\ v_m \end{bmatrix}^T \tag{22}$$

B. Data-Driven Nonlinear Control Design

The structure of the control system is depicted in Fig. 5. As it can be observed, the diagram includes the DER model, inner current and voltage regulators to be designed using feedback linearization theory, and output power controller. The transfer function of the DER model can be obtained via the proposed data-driven SINDy. For this purpose, the obtained SINDy model $\dot{\mathbf{X}} = \mathbf{\Theta}(\mathbf{X}, \mathbf{U})$ is re-arranged into the original form represented by (7). The transfer function is then obtained from the state-space model, details of which can be found in [13]. Power and voltage regulation at the PCC are the control objectives. As a result, the nonlinear controller regulates the output power through an outer loop control input and regulates the voltage through an inner loop control input. In this design, the main objective of the controller is to regulate voltage instead of reactive power at the point of common coupling. This is mainly because VSCs suffer from voltage stability issues when tied to a grid with high penetration of DERs, which is why it was recommended in [34] to maintain the AC voltage level at the PCC instead of reactive power control. The measured active power of the DER at the PCC, p_m, will pass through a low-pass filter with the bandwidth of ω_c, therefore, the dynamics of active power measurement can be expressed as:

$$\dot{p}_m = -\omega_c p_m + 1.5(v_{pd} i_{nd} + v_{pq} i_{nq})\omega_c \tag{23}$$

To regulate the output power of the DER, the active power tracking error $(p^* - p_m)$ will be passed through a compensator $G_P(s)$ that generates the converter voltage angle, δ. The converter angle along with the nominal magnitude of the AC voltage, V_{nom}, are then used to generate the dq-frame reference voltages, v_{pd}^* and v_{pq}^*, according to:

$$\delta^* = \left(k_p + \frac{k_i}{s}\right)(p^* - p_m) = G_p(s)(p^* - p_m) \tag{24}$$

$$v_{pd}^* = V_{nom}\cos(\delta^*) \qquad v_{pq}^* = V_{nom}\sin(\delta^*) \tag{25}$$

where $G_p(s) = \left(k_p + \dfrac{k_i}{s}\right)$ is a proportional integral (PI) regulator for active power control of the DER.

C. Inner Control Design using Feedback Linearization

The inner controllers include voltage and current regulators, which will be designed using feedback linearization theory and will be tested on the obtained data-driven DER model.

1) Inner Voltage Controller: The voltage regulator tries to minimize the voltage tracking error, i.e., $e_{vd} = v_{pd}^* - v_{pd}$ and $e_{vq} = v_{pq}^* - v_{pq}$. According to the feedback linearization theory, we need to first find the derivative of the voltage tracking errors (i.e., $\dot{e}_{vd} = \dot{v}_{pd}^* - \dot{v}_{pd}$ and $\dot{e}_{vq} = \dot{v}_{pq}^* - \dot{v}_{pq}$). Next, by replacing $\dot{v}_{pd}$ and $\dot{v}_{pq}$ from (5) and (6), voltage tracking dynamics is expressed as:

$$\dot{e}_{vd} = \dot{v}_{pd}^* + \frac{1}{C_f}(i_{nd} - i_{cd}) - \omega_0 v_{pq} \tag{26}$$

$$\dot{e}_{vq} = \dot{v}_{pq}^* + \frac{1}{C_f}(i_{nq} - i_{cq}) + \omega_0 v_{pd} \tag{27}$$

To decouple the dynamics in dq frame, we will first define $g(e_{vd}) = \dfrac{1}{C_f} i_{nd} - \omega_0 v_{pq} + \dot{v}_{pd}^*$ and $g(e_{vq}) = \dfrac{1}{C_f} i_{nq} + \omega_0 v_{pd} + \dot{v}_{pq}^*$ to simplify the voltage tracking dynamics to $\dot{e}_{vd} = g(e_{vd}) - \dfrac{1}{C_f} i_{cd}$ and $\dot{e}_{vq} = g(e_{vq}) - \dfrac{1}{C_f} i_{cq}$. By defining $[\dot{e}_{vd}, \dot{e}_{vd}] = [\dot{y}_1, \dot{y}_2]$, the above equation can be written in a matrix form as:

$$\begin{bmatrix} \dot{y}_1 \\ \dot{y}_2 \end{bmatrix} = \begin{bmatrix} L_1 h_1(x) \\ L_1 h_2(x) \end{bmatrix} - \frac{1}{C_f} \begin{bmatrix} i_{cd} \\ i_{cq} \end{bmatrix} \tag{28}$$

where $L_1 h_1(\mathbf{x}) = g(e_{vd})$, and $L_1 h_2(\mathbf{x}) = g(e_{vq})$. Looking at the above equation and comparing it with the input design for the feedback linearization theory expressed in (21), it is observed that $E_{vd}^{-1}(x) = E_{vq}^{-1}(x) = -\dfrac{1}{C_f} \longrightarrow E_{vd}^{-1}(x) = -C_f$, one can design the control inputs $u = [i_{cd}^*, i_{cq}^*]$ referring to (21) as $-E^{-1}(x)\left(\begin{bmatrix} L_1 h_1(x) \\ L_1 h_2(x) \end{bmatrix} + \begin{bmatrix} v_1 \\ v_2 \end{bmatrix}\right)$, which is simplified to:

$$i_{cd}^* = C_f\left[-g(e_{vd}) + v_1\right] = G_{vd}(s) e_{vd} \tag{29}$$

$$i_{cq}^* = C_f\left[-g(e_{vq}) + v_2\right] = G_{vq}(s) e_{vq} \tag{30}$$

where v_1 and v_2 are two new inputs to regulate the voltage tracking error to zero. In the above equations, G_{vd} and G_{vq} can be calculated by:

$$G_{vd}(s) = C_f\left[\left(K_1 + \frac{K_2}{s}\right) - \frac{g(e_{vd})}{e_{vd}}\right] \tag{31}$$

$$G_{vq}(s) = C_f\left[\left(K_1 + \frac{K_2}{s}\right) - \frac{g(e_{vq})}{e_{vq}}\right] \tag{32}$$

where $v_1 = (K_1 + \dfrac{K_2}{s}) e_{vd}$ and $v_2 = (K_1 + \dfrac{K_2}{s}) e_{vq}$ are two PI regulators to force the voltage dynamics to zero.

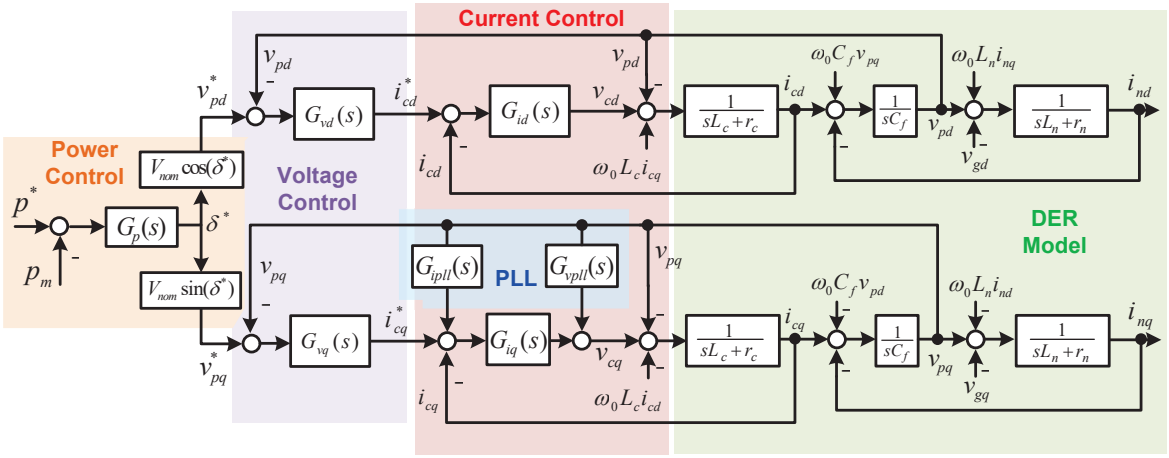

Fig. 5: Block diagram of the proposed data-driven DER control with feedback linearization technique.

2) Inner Current Controller: Next, to limit the converter current during faults and contingencies, an inner current controller needs to be developed utilizing the current tracking error, which is denoted by $e_{id} = i^*_{cd} - i_{cd}$ and $e_{iq} = i^*_{cq} - i_{cq}$. Similar to the voltage controller design and following the feedback linearization theory, the derivative of current tracking error will be obtained (i.e., $\dot{e}_{id} = \dot{i}^*_{cd} - \dot{i}_{cd}$ and $\dot{e}_{iq} = \dot{i}^*_{cq} - \dot{i}_{pcq}$). By replacing the dynamics of dq frame converter current, e.g., $\dot{i}_{cd}$ and $\dot{i}_{cq}$, from (1) and (2), the current tracking dynamics is expressed as:

$$\dot{e}_{id} = \dot{i}^*_{cd} + \frac{r_c}{L_c} i_{cd} - \omega_0 i_{cq} + \frac{1}{L_c}(v_{cd} - v_{pd}) \tag{33}$$

$$\dot{e}_{iq} = \dot{i}^*_{cq} + \frac{r_c}{L_c} i_{cq} + \omega_0 i_{cd} + \frac{1}{L_c}(v_{cq} - v_{pq}) \tag{34}$$

By defining $g(e_{id}) = \dot{i}^*_{cd} + \frac{r_c}{L_c} i_{cd} - \omega_0 i_{cq} - \frac{1}{L_c} v_{pd}$, and $g(e_{iq}) = \dot{i}^*_{cq} + \frac{R_c}{L_c} i_{cq} + \omega_0 i_{cd} - \frac{1}{L_c} v_{pq}$, the above equations simplify to: $\dot{e}_{id} = g(e_{id}) + \frac{1}{L_c} v_{cd}$ and $\dot{e}_{iq} = g(e_{iq}) + \frac{1}{L_c} v_{cq}$. Then, using the control design law from the feedback linearization theory in (21), the converter voltage control inputs can be defined using a proportional controller K_3 as:

$$v_{cd} = -L_c g(e_{id}) + L_c K_3 e_{id} = G_{id}(s) e_{id} \tag{35}$$

$$v_{cq} = -L_c g(e_{iq}) + L_c K_3 e_{iq} = G_{iq}(s) e_{iq} \tag{36}$$

D. Impact of Phase-locked Loop

By measuring the voltage at the PCC and forcing the q component of the PCC voltage to zero, phase-locked loop (PLL) provides the transformation angle for dq-frame conversion denoted by $\theta_{pll}(t) = \omega t$. The PLL's closed-loop transfer function is obtained by [35]:

$$G^{pll}_c(s) = \frac{\Delta\theta_{pll}(s)}{\Delta v_{pq}(s)} = \frac{G_{pll}(s)}{s + G_{pll}(s) V_{pd}} \tag{37}$$

where $G_{pll}(s) = k^{pll}_p + \frac{k^{pll}_i}{s}$ is a PI regulator to force the q-component of PCC voltage to zero, and V_{pd} denotes the voltage amplitude at the PCC. According to [35], [36], the impact of PLL on the control structure of the DER is studied by supplementing two terms including $\Delta I_{pll}(s) = -\Delta\theta_{pll}(s) I_{cd0}$ to the reference converter current in q frame and $\Delta V_{pll}(s) = \Delta\theta_{pll}(t) V_{pd0}$ to the reference converter voltage in the q frame. By replacing $\Delta\theta_{pll}(s)$ from (37) in these feedforward items, the PLL dynamics are expressed as:

$$\Delta I_{pll}(s) = -G^{pll}_c(s) I_{cd0} \Delta v_{pq} = G_{ipll}(s) \Delta v_{pq}(s) \tag{38}$$

$$\Delta V_{pll}(s) = G^{pll}_c(s) V_{pd0} \Delta v_{pq} = G_{vpll}(s) \Delta v_{pq}(s) \tag{39}$$

which will be added to the overall control block diagram of the converter as illustrated in Fig. 5. The block diagram of the closed-loop control of the DER with data-driven nonlinear controller will be used for stability analysis purposes. Fig. 6 depicts the detailed implementation of the proposed data-driven control.

V. Case Studies

To validate the effectiveness of the proposed model-free nonlinear DER control in the grid-tied mode, several case studies are carried out using time-domain simulations and eigenvalue analysis in MATLAB. The DER parameters used for time-domain simulations are obtained from [13].

A. Sensitivity Analysis

To analyze the impact of the proposed data-driven DER control on the stability of the system, eigenvalue analysis is carried out to compare the data-driven DER control with a model-based control. Two block diagram of the DER controller shown in Fig. 5 were developed in MATLAB/Simulink, one using an actual model represented by (7) and the other one using the SINDy model. Next, the "LINMOD" function of MATLAB was used to derive the state-space linearized A, B, C, D matrices of the closed-loop system for eigenvalue analysis. Table I illustrates a detailed comparison between the eigenvalues of the actual model and the proposed data-driven model. As it can be observed, the system has 12 eigenvalues with detailed participation factor analysis shown in the X_{pf} column that relates the modes to the state variables of the

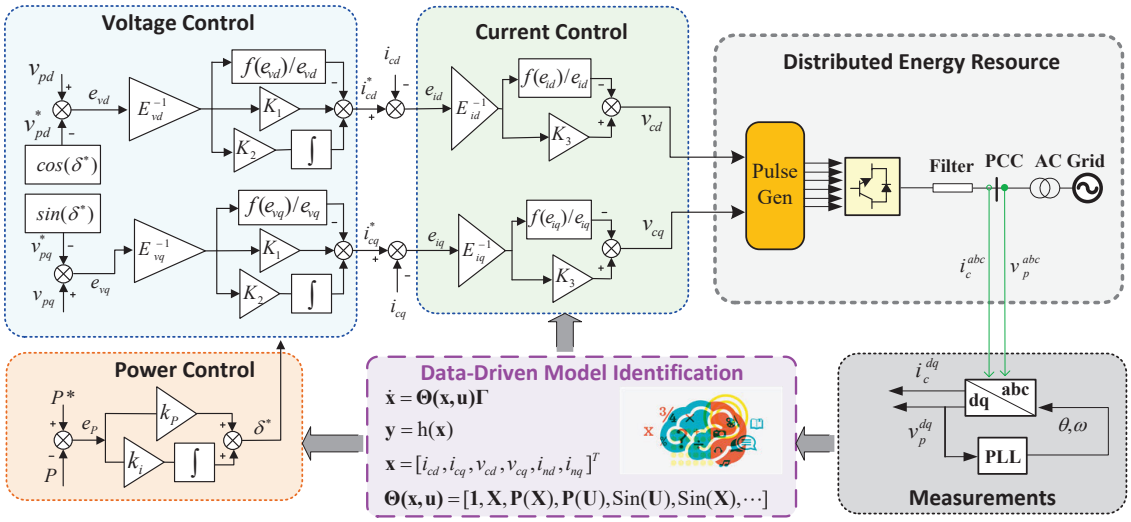

Fig. 6: Implementation of the proposed data-driven DER control using feedback linearization theory.

TABLE I: Eigenvalue comparison of the physical DER controller with the data-driven one.

	Actual			Data-Driven		
X_{pf}	λ	f (Hz)	η (%)	λ	f (Hz)	η (%)
$p_m, \omega, v_{cd}, i_{cd}$	$\lambda_1 = -4.3 + j2037$	324	0.21	$\lambda_1 = -4.4 + j2778$	442	0.15
$p_m, \omega, v_{cd}, i_{cd}$	$\lambda_2 = -4.3 - j2037$	324	0.21	$\lambda_2 = -4.4 - j2788$	442	0.15
p_m, ω	$\lambda_3 = -2.2 + j1283$	204	0.17	$\lambda_3 = -1.5 + j1524$	242	0.1
p_m, ω	$\lambda_4 = -2.2 - j1283$	204	0.17	$\lambda_4 = -1.5 - j1524$	242	0.1
θ, γ_P	$\lambda_5 = -1.3 + j377$	60	0.34	$\lambda_5 = -1.2 + j377$	60	0.34
θ, γ_P	$\lambda_6 = -1.3 - j377$	60	0.34	$\lambda_6 = -1.2 - j377$	60	0.34
v_{cd}	$\lambda_7 = -56.6$	0	100	$\lambda_7 = -56.6$	0	100
i_{cq}	$\lambda_8 = -6.96$	0	100	$\lambda_8 = -7.25$	0	100
i_{nq}	$\lambda_9 = -0.1$	0	100	$\lambda_9 = -0.1$	0	100
i_{nd}	$\lambda_{10} = -8.5e^{-6}$	0	100	$\lambda_{10} = -4.9e^{-6}$	0	100
v_{pq}	$\lambda_{11} = -8.5e^{-6}$	0	100	$\lambda_{11} = -4.7e^{-6}$	0	100
v_{pd}	$\lambda_{12} = -8.5e^{-6}$	0	100	$\lambda_{12} = -4.7e^{-6}$	0	100

system. Each mode's frequency and damping are also listed in the table. As shown in the Table, the data-driven eigenvalues closely match the actual ones, indicating the effectiveness of the proposed data-driven model and control design for stability analysis in smart grids. As can be observed in both cases, all modes reside in the left half-plane (LHP) and the system is stable. In the case studies, we will investigate the impact of system parameters on these eigenvalues.

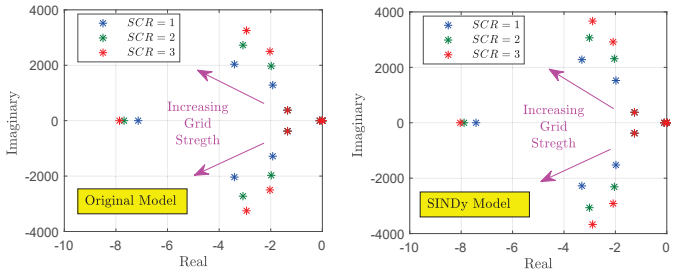

Fig. 7: Impact of grid weakness on eigenvalues.

1) Impact of Grid Strength: To analyze the sensitivity of the proposed data-driven DER controller in various AC grid conditions, three short circuit ratios (SCRs) are considered, where SCR=1 represents a very weak AC grid (or ultra weak AC grid), SCR=2 represents a weak AC grid, and SCR=3 is a strong grid. The eigenvalues of the original model (actual model) and the data-driven SINDy are compared for these three grid integration case studies and the trajectory of eigenvalues is plotted in Fig. 7. First, the results show a good match between the trajectory of the eigenvalues in the proposed data-driven DER control (SINDy) and the model-based DER control (original model). Furthermore, it is observed that by reducing the strength of the AC grid, the eigenvalues move towards the right half-plane (RHP), but the system remains stable thanks to the superiority of feedback linearized controller.

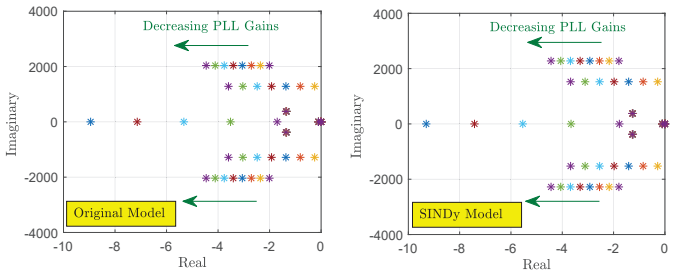

Fig. 8: Impact of PLL gains on eigenvalues.

2) Impact of Control Parameters: To analyze whether the proposed data-driven DER control can accurately track the trajectory of eigenvalues when the parameters of the controller change, the impact of PLL gains on stability of the designed controller was studied as shown in Fig. 8. By modifying the PLL gains in both proposed data-driven and actual DER control, the trajectory of the eigenvalues were plotted. It can be observed that by increasing the PLL gains, four eigenvalues move towards the origin denoting the increase in the PLL gains might destabilize the system. A comparison of the trajectory of the eigenvalues in a data-driven DER model (right subplot) and a physical model (left subplot) shows a close agreement between the two models, indicating that the proposed data-driven model can be successfully used for smart grid stability analysis.

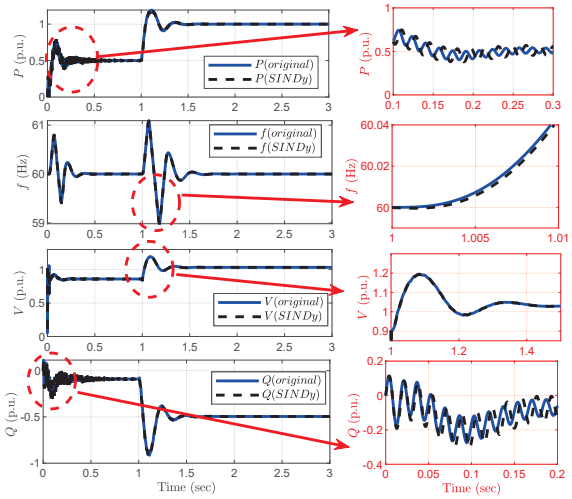

Fig. 9: Simulation results for weak AC grid integration of the proposed data-driven DER control.

B. Time-domain Simulations

To validate the effectiveness of the designed feedback-linearization-based nonlinear controller, time-domain simulations on a grid-connected converter are carried out using MATLAB Simscape power system toolbox. Three case studies are considered: (1) DER's active power response when the AC grid is (ultra weak) (SCR=1), (2) black-start capability of the proposed data-driven DER controller when SCR=1, and (3) microgrid integration of the proposed data-driven DER control.

1) DER's Active Power Response: Fig. 9 shows the comparison results for capability of a data-driven DER control and a model-based DER control in transferring an active power of 1 p.u. in an (ultra weak) weak AC grid with SCR=1. The active power setpoint of the converter is first set to 0.5 p.u., which is increased to 1 p.u. at $t = 1$ sec. Using SINDy, a data-driven DER controller is shown to successfully deliver 1 p.u. active power in an (ultra weak) weak AC grid condition with SCR=1. In addition, as the figure confirms, the trajectory of system states including active power, frequency, voltage magnitude, and reactive power in a data-driven DER closely matches that of a physical model. The results confirm the success of the proposed data-driven framework for DER control in weak AC grid scenarios.

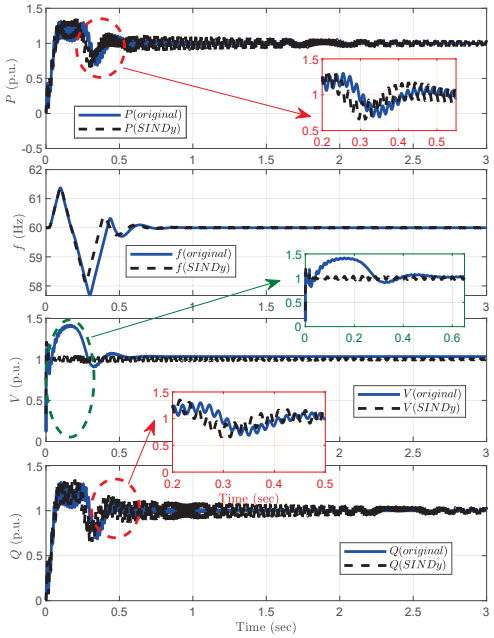

Fig. 10: Simulation results for blackstart capability of the proposed data-driven DER control.

2) Black-start Capability: This case examines the capability of proposed data-driven DER controller in a black-start scenario. To test the black-start capability, the reference active power of the DER is suddenly changed from 0 to 1 p.u. at $t = 0$ sec and the simulation results are shown in Fig. 10. As it can be observed, a feedback linearization controller can successfully deliver 1 p.u. of active power from a black-start condition. In addition, the trajectory of the system states in the proposed data-driven model based on SINDy closely matches that of the DER control that was designed using a detailed physical model. Therefore, a data-driven control design using SINDy proves to be effective for blackstart conditions.

3) Microgrid Operation: To study whether the data-driven DER control can perform as expected in the islanded mode, the proposed data-driven DER controller was tested in a microgrid. The microgrid model is composed of a DER with the proposed data-driven feedback linearization controller and three solar photovoltaic (PV) plants, all of which are connected to the AC grid through the point of common coupling depicted in Fig. 11. Through a three-phase VSC and a filter, each solar array is connected to the PCC. Vector control in the synchronous reference frame is used with maximum power point tracking (MPPT) to control the solar inverters. The PV systems operate at a constant solar irradiance input of $900W/m^2$ supplemented with random noise to account for the uncertain behavior of the output PV power. More information on developing the solar photovoltaic system can be found in [37], [38].

Simulation results for microgrid integration of the nonlinear controlled VSC is demonstrated in Fig. 12, where the last subplot depicts the aggregated solar PV power that averages

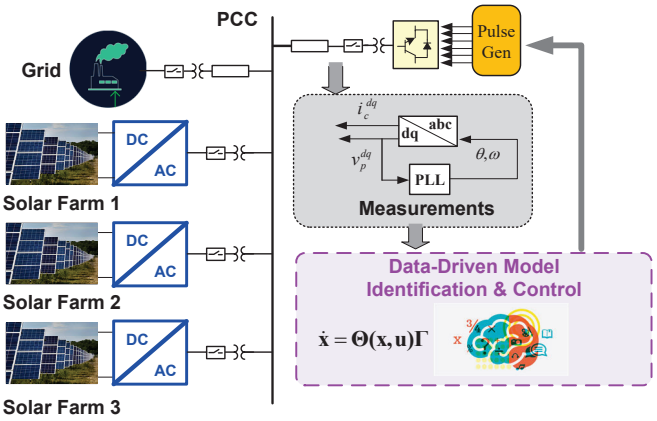

Fig. 11: Microgrid integration of the proposed controller.

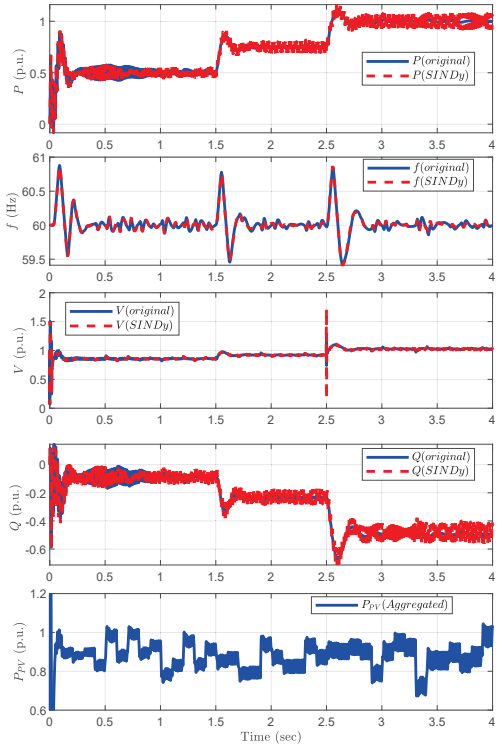

Fig. 12: Simulation results for fault ride through capability of nonlinear-based controller when SCR=1.

around 0.9 p.u. The active power reference of the data-driven DER was set to 0.5 p.u. initially, which was increased to 0.75 at $t = 1.5$ sec and to 1 p.u. at $t = 2.5$ sec. It is evident that PV farms' output is highly uncertain due to irradiance variations. There were a few spikes in voltage and frequency at the PCC as a result of the intermittency of the solar farm. Comparing the trajectory of the states in the data-driven DER and the original DER using physical model, one can confirm the close match between the two. It is observed that the proposed data-driven control of DERs using SINDy can successfully operate when controlling DERs that are integrated to the grid or a microgrid with high penetration of renewables. Therefore, data-driven nonlinear control frameworks open up new possibilities for accurate control with performance guarantees in smart grid applications, which would otherwise be very challenging. It is noted that since the control design is usually carried out for individual DERs and the control algorithm is embedded in the inverter of the DER before integrating it to the grid, model identification also needs to be carried out before integrating the DER to the grid. In addition, since the prediction is very close to real parameters (physics-based model), the control gains in the data-driven design are fairly close to the control gains in physics-based models. Therefore, as confirmed by simulation results, even if there are multiple DERs operating in parallel, the proposed data-driven control can successfully achieve the control objectives.

C. Real-time Verification

The active power response scenario for the proposed data-driven method in Section V-B is replicated in real time using the OPAL-RT real-time testbed shown in Fig. 13. To this end, first the grid-connected DER with the SINDy-based control is built in Simulink® and compiled in RT-LAB. The model is then executed on one of the CPU cores of the OP4510 real-time target and is controlled through a TCP/IP link by the Simulink® GUI running on the host PC. Desired measurements are then sent to a digital oscilloscope in real-time via the analog outputs of the OP4510 target.

As can be seen from Fig. 14, the waveforms obtained for P, f, V, and Q using the SINDy-based control that is run in real time, closely follow their offline simulation counterparts shown in Fig. 9. The real-time results also exhibit close trajectories to the detailed physics-based design, verifying the capability of the proposed method for implementation in real time.

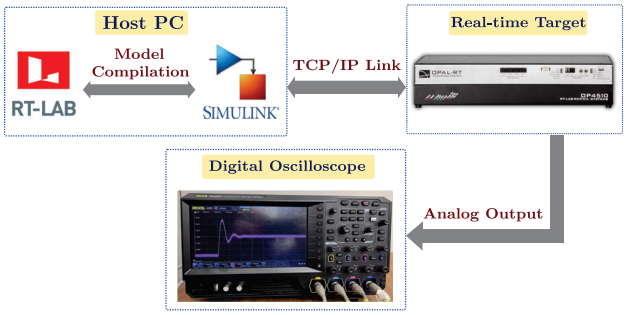

Fig. 13: Real-time testbed configuration.

VI. Conclusion

In this paper, a model-free nonlinear control of DERs using feedback linearization technique was studied. Using the sparse identification of nonlinear dynamics with control that utilized the available measurements from the point of common coupling of DERs to the grid, dynamics of the DER were predicted by leveraging a library of candidate functions. The learned dynamics were then used to develop control designs for voltage regulation, active power regulation, and current control of DERs using the feedback linearization technique. The proposed research demonstrates the effectiveness of sparse

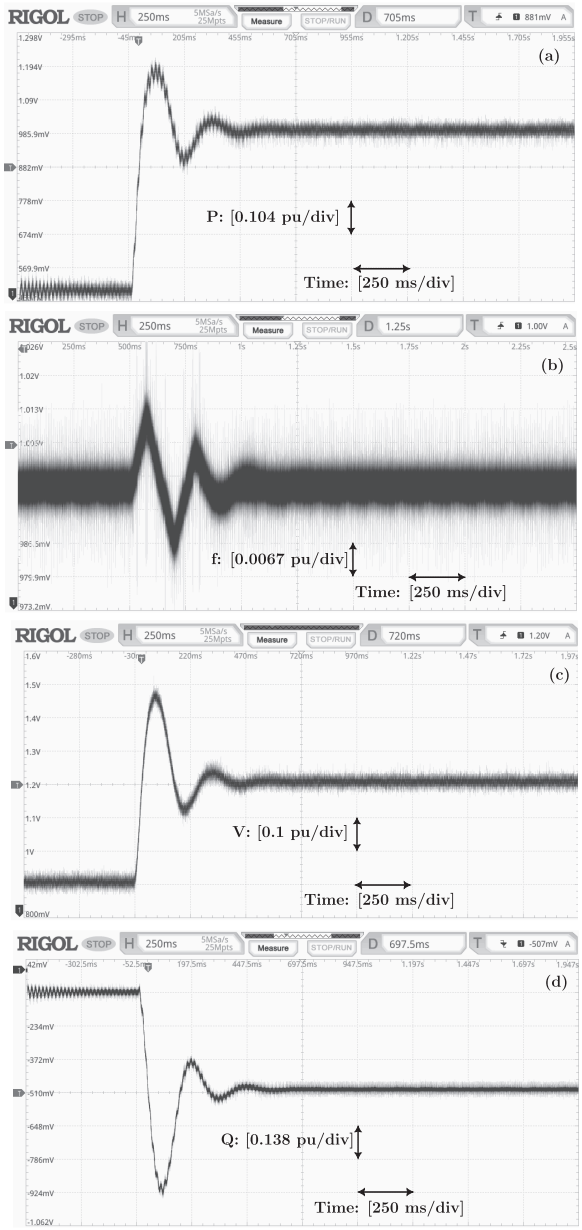

Fig. 14: Real-time verification of the proposed data-driven DER control. (a) P (p.u.), (b) f (p.u.), (c)V (p.u.), and (d) Q (p.u.).

identification for data-driven model identification of nonlinear DER systems and successfully tracking the dynamic trajectory of DER states during contingencies or operating point changes. We also demonstrated the effectiveness of the proposed data-driven approach for stability analysis of DERs in smart grids, which could significantly reduce the complexities of existing model-based stability analysis approaches. We showed that without having a physical model, complex dynamics of DERs can be identified using measurements and the data-driven model can be utilized for nonlinear control designs that could provide stability guarantees and robustness in smart grid applications. Such formulation can significantly reduce the existing complexities of control design in smart grid. One of the main challenges of utilizing SINDy for model identification of DERs is that it requires some initial knowledge about the DER dynamics as randomly generating the library of candidate functions and increasing the components of library functions can reduce the prediction accuracy. In the future work, we will explore other techniques such as deep learning to learn the best candidate functions that could be applied for DER model identification using SINDy.

REFERENCES

[1] L. Fan and Z. Miao, "Admittance-based stability analysis: Bode plots, nyquist diagrams or eigenvalue analysis?" *IEEE Transactions on Power Systems*, vol. 35, no. 4, pp. 3312–3315, 2020.

[2] Y. Peng, Z. Shuai, X. Liu, Z. Li, J. M. Guerrero, and Z. J. Shen, "Modeling and stability analysis of inverter-based microgrid under harmonic conditions," *IEEE Transactions on Smart Grid*, vol. 11, no. 2, pp. 1330–1342, 2019.

[3] B. Liu, Q. Wei, C. Zou, and S. Duan, "Stability analysis of lcl-type grid-connected inverter under single-loop inverter-side current control with capacitor voltage feedforward," *IEEE Transactions on Industrial Informatics*, vol. 14, no. 2, pp. 691–702, 2017.

[4] A. Firdaus and S. Mishra, "Auxiliary signal-assisted droop-based secondary frequency control of inverter-based pv microgrids for improvement in power sharing and system stability," *IET Renewable Power Generation*, vol. 13, no. 13, pp. 2328–2337, 2019.

[5] P. Piya, M. Ebrahimi, M. Karimi-Ghartemani, and S. A. Khajehoddin, "Fault ride-through capability of voltage-controlled inverters," *IEEE Transactions on Industrial Electronics*, vol. 65, no. 10, pp. 7933–7943, 2018.

[6] A. Firdaus and S. Mishra, "Mitigation of power and frequency instability to improve load sharing among distributed inverters in microgrid systems," *IEEE Systems Journal*, vol. 14, no. 1, pp. 1024–1033, 2019.

[7] L. Zhang, L. Harnefors, and H. Nee, "Power-synchronization control of grid-connected voltage-source converters," *IEEE Trans. Power Syst.*, vol. 25, no. 2, pp. 809–820, May 2010.

[8] W. J. Farmer and A. J. Rix, "Optimising power system frequency stability using virtual inertia from inverter-based renewable energy generation," *IET Renewable Power Generation*, vol. 14, no. 15, pp. 2820–2829, 2020.

[9] Z. Wang, F. Zhuo, H. Yi, J. Wu, F. Wang, and Z. Zeng, "Analysis of dynamic frequency performance among voltage-controlled inverters considering virtual inertia interaction in microgrid," *IEEE Transactions on Industry Applications*, vol. 55, no. 4, pp. 4135–4144, 2019.

[10] H. Makhamreh, M. Trabelsi, O. Kükrer, and H. Abu-Rub, "An effective sliding mode control design for a grid-connected puc7 multilevel inverter," *IEEE Transactions on Industrial Electronics*, vol. 67, no. 5, pp. 3717–3725, 2019.

[11] C. D. Townsend, G. Mirzaeva, and G. C. Goodwin, "Deadtime compensation for model predictive control of power inverters," *IEEE Transactions on Power Electronics*, vol. 32, no. 9, pp. 7325–7337, 2016.

[12] R. Errouissi, S. Muyeen, A. Al-Durra, and S. Leng, "Experimental validation of a robust continuous nonlinear model predictive control based grid-interlinked photovoltaic inverter," *IEEE Transactions on Industrial Electronics*, vol. 63, no. 7, pp. 4495–4505, 2015.

[13] J. Khazaei, Z. Tu, A. Asrari, and W. Liu, "Feedback linearization control of converters with lcl filter for weak ac grid integration," *IEEE Transactions on Power Systems*, vol. 36, no. 4, pp. 3740–3750, 2021.

[14] J. Iqbal, M. Ullah, S. G. Khan, B. Khelifa, and S. Ćuković, "Nonlinear control systems-a brief overview of historical and recent advances," *Nonlinear Engineering*, vol. 6, no. 4, pp. 301–312, 2017.

[15] R. Sepulchre, M. Jankovic, and P. V. Kokotovic, *Constructive nonlinear control*. Springer Science & Business Media, 2012.

[16] H. J. Marquez, *Nonlinear control systems: analysis and design*. Wiley-Interscience Hoboken, NJ, 2003, vol. 1.

[17] M. Liu, L. Tan, and S. Cao, "Method of dynamic mode decomposition and reconstruction with application to a three-stage multiphase pump," *Energy*, vol. 208, p. 118343, 2020.

[18] T. Qin, K. Wu, and D. Xiu, "Data driven governing equations approximation using deep neural networks," *Journal of Computational Physics*, vol. 395, pp. 620–635, 2019.

[19] M. Al-Gabalawy, "Deep learning for koopman operator optimal control," *ISA transactions*, 2021.

[20] U. Fasel, E. Kaiser, J. N. Kutz, B. W. Brunton, and S. L. Brunton, "Sindy with control: A tutorial," *arXiv preprint arXiv:2108.13404*, 2021.

[21] G. Kandaperumal, K. P. Schneider, and A. K. Srivastava, "A data-driven algorithm for enabling delay tolerance in resilient microgrid controls using dynamic mode decomposition," *IEEE Transactions on Smart Grid*, vol. 13, no. 4, pp. 2500–2510, 2022.

[22] J. Bedi and D. Toshniwal, "Empirical mode decomposition based deep learning for electricity demand forecasting," *IEEE access*, vol. 6, pp. 49 144–49 156, 2018.

[23] M. Netto and L. Mili, "A robust data-driven koopman kalman filter for power systems dynamic state estimation," *IEEE Transactions on Power Systems*, vol. 33, no. 6, pp. 7228–7237, 2018.

[24] Y. Hirase, Y. Ohara, N. Matsuura, and T. Yamazaki, "Dynamics analysis using koopman mode decomposition of a microgrid including virtual synchronous generator-based inverters," *Energies*, vol. 14, no. 15, p. 4581, 2021.

[25] K. A. Severson, P. M. Attia, N. Jin, N. Perkins, B. Jiang, Z. Yang, M. H. Chen, M. Aykol, P. K. Herring, D. Fraggedakis *et al.*, "Data-driven prediction of battery cycle life before capacity degradation," *Nature Energy*, vol. 4, no. 5, pp. 383–391, 2019.

[26] Y. Li, Y. Liao, X. Wang, L. Nordström, P. Mittal, M. Chen, and H. V. Poor, "Neural network models and transfer learning for impedance modeling of grid-tied inverters," in *2022 IEEE 13th International Symposium on Power Electronics for Distributed Generation Systems (PEDG)*. IEEE, 2022, pp. 1–6.

[27] S. L. Brunton, J. L. Proctor, and J. N. Kutz, "Discovering governing equations from data by sparse identification of nonlinear dynamical systems," *Proceedings of the National Academy of Sciences*, vol. 113, no. 15, pp. 3932–3937, 2016.

[28] A. Mauroy, I. Mezić, and Y. Susuki, *The Koopman Operator in Systems and Control: Concepts, Methodologies, and Applications*. Springer Nature, 2020, vol. 484.

[29] S. L. Brunton, J. L. Proctor, and J. N. Kutz, "Discovering governing equations from data by sparse identification of nonlinear dynamical systems," *Proceedings of the national academy of sciences*, vol. 113, no. 15, pp. 3932–3937, 2016.

[30] ——, "Sparse identification of nonlinear dynamics with control (sindyc)," *IFAC-PapersOnLine*, vol. 49, no. 18, pp. 710–715, 2016.

[31] S. Larsson and V. Thomée, *Partial differential equations with numerical methods*. Springer, 2003, vol. 45.

[32] L. Zhang and H. Schaeffer, "On the convergence of the sindy algorithm," *Multiscale Modeling & Simulation*, vol. 17, no. 3, pp. 948–972, 2019.

[33] A. Isidori, *Nonlinear control systems*. Springer Science & Business Media, 2013.

[34] L. Zhang, L. Harnefors, and H.-P. Nee, "Power-synchronization control of grid-connected voltage-source converters," *IEEE Trans. Power Syst.*, vol. 25, no. 2, pp. 809–820, 2009.

[35] B. Wen, D. Boroyevich, R. Burgos, P. Mattavelli, and Z. Shen, "Analysis of DQ small-signal impedance of grid-tied inverters," *IEEE Trans. Power Electron.*, vol. 31, no. 1, pp. 675–687, 2015.

[36] Y. Tang, J. Fang, X. Li, and H. Li, "Reshaping quadrature-axis impedance of three-phase grid-connected converters for low-frequency stability improvement," in *2018 International Power Electronics Conference (IPEC-Niigata 2018-ECCE Asia)*. IEEE, 2018, pp. 3910–3915.

[37] J. Khazaei, Z. Miao, L. Piyasinghe, and L. Fan, "Real-time digital simulation-based modeling of a single-phase single-stage PV system," *Electric Power Systems Research*, vol. 123, pp. 85–91, 2015.

[38] J. Khazaei, Z. Tu, and W. Liu, "Small-Signal Modeling and Analysis of Virtual Inertia-based PV Systems," *IEEE Trans. Energy Convers.*, 2020.

Javad Khazaei (S'10 M'16 SM'20) received the Ph.D. degree in Electrical Engineering from University of South Florida (USF) in 2016 with focus on power and energy systems. He is currently an Assistant Professor at the Electrical and Computer Engineering Department at Lehigh University, PA, USA. His research interests include data-driven and model-based control, optimization, and dynamic modeling of cyber-physical power systems and microgrids, smart grid security, and power electronics applications in smart grids and shipboard microgrids.

Ali Hosseinipour (S'21) received the B.S. and M.S. degrees in electrical engineering from Shahid Bahonar University of Kerman, Iran. Currently, he is pursuing a Ph.D. in electrical engineering at the Electrical and Computer Engineering Department at Lehigh University, PA, USA. His research interests include dynamic modeling and control of modern power systems and microgrids.

In 2023, he received an IEEE Graduate Student Poster Award for his work on data-driven impedance modeling of power converters in microgrids at the IEEE 2023 Power and Energy Society General Meeting.